 doi:10.20944/preprints202209.0022.v1

Article

Application of Composite Variable Structure PI in the IPMSM Speed Sensorless Control System

Weidong Feng [1], Jing Bai [2,*], Zhiqiang Zhang [3] and Jing Zhang [4]

[1] College of Electrical and Information Engineering, Beihua University, Ji Lin 132013, China; 15990730899@163.com
[2] College of Electrical and Information Engineering, Beihua University, Ji Lin 132013, China
[3] Power Supply Company, Bao Tou 014000, China; 18686108186@163.com
[4] College of Electrical and Information Engineering, Beihua University, Ji Lin 132013, China; 2621002294@qq.com
* Correspondence: jlbyj@163.com

Abstract: In the speed control system of Interior Permanent Magnet Synchronous Motor (IPMSM) without a speed sensor, the speed under the traditional PI control suffers from poor tracking performance and step response overshoot. This paper proposes a Compound Variable Structure PI (CVSPI) controller to improve the system control performance. It can choose whether to include an integral term according to the size of the system deviation to speed up the response. It also introduces a Model Reference Adaptive System (MRAS) speed observer in the controller to estimate the speed and adaptively adjust the size of the anti-integration saturation gain to improve the dynamic response following performance and immunity of the system. A feed-forward link is added for a given input differential to achieve an accurate answer to time-varying inputs. As the linear compensation matrix of the conventional MRAS is a unit matrix, the speed can only be accurately observed in a specific speed range. In this paper, a new linear compensation matrix is designed, and a new speed adaptive law is derived, allowing the improved MRAS to measure speed over a wide range accurately. Simulation results validate the excellent control performance of the CVSPI and the accuracy of the enhanced MRAS over a wide speed range.

Keywords: composite variable structure PI; Interior Permanent Magnet Synchronous Motor; improved MRAS

1. Introduction

Interior Permanent Magnet Synchronous Motor (IPMSM) is widely used in industrial speed control systems for its high power/weight ratio, high torque/inertia ratio, high efficiency, and certain robustness [1-3]. Although a range of superior and complicated control techniques such as non-linear PI control [4], adaptive control, and sliding mode variable shape control has been utilized in the velocity loop [5], these non-linear control techniques have issues such as hard parameter adjustment or jitter. They need to be further improved [6]. Therefore, the dominant control method in industrial applications is still traditional PI control [7-9]. The conventional PI control is designed based on linear system theory [10], and a fixed set of PI parameters will cause a contradiction between the system's steady-state performance and dynamic performance [11], making it difficult to take into account the steady-state performance and dynamic performance of the system at the same time [12]. Due to the physical constraints of the motor and inverter, limits must be placed on the system control inputs to protect the system [13]. When the controller output is limited by saturation due to an increase in the accumulation of the integral term (as can happen when there is a step response or sudden changes in load), a phenomenon known as Windup occurs [14-16]. This leads to a decline in the performance of the closed-loop system (e.g., a larger overshoot, a longer regulation time, and even the system losing stability). Therefore, the traditional PI controller can no longer meet the requirements of

 doi:10.20944/preprints202209.0022.v1

industrial automation for time-varying speed tracking and robustness in real-time [17]. At the same time, the actual speed feedback in a closed loop system is mainly obtained indirectly by differentiating the mechanical angle of the rotor detected by the position sensor [18]. The installation of position sensors increases the motor's size, and cost increases the rotor's inertia [19,20], is prone to failure in complex environments, affects the dynamic and static performance of the system, and reduces the system's robustness [21]. Therefore, the use of position sensors needs to be abandoned, and a speed sensor-less control strategy adopted to enhance the closed-loop system's performance and the speed feedback's accuracy [22].

In [23], a variable gain PI controller is proposed to automatically select the optimum gain for a given rate of change and thus achieve good speed tracking performance. However, as the gain of the PI controller changes in real-time, it is impossible to avoid the fluctuation of the system speed for a given speed change. To improve the system's performance against external load disturbances, [24] uses a non-linear disturbance observer to estimate the load torque and then adaptively adjust the fractional order PI parameters. Although this method is effective, the design process requires consideration of many non-ideal factors, and the algorithm is complex and not very practical. After analyzing the link between PI controller parameters and zero poles of the system, [25] proposes a PI controller parameter modification approach based on the pole arrangement that effectively dampens mechanical vibration when operating with flexible loads. However, the PI parameter tuning in this method only addresses the mechanical vibration problem of the system, and the tracking performance of the continuously changing input of the system has not been considered. [26] introduces an active disturbance rejection controller (ADRC) for speed regulation to compensate for disturbances inside and outside the IPMSM. Still, the parameter tuning of the ADRC is too tricky, and the tracking performance for different states of speed given is not universal. In [27], a fast super-distortion algorithm is proposed for the poor robustness of PI controllers in speed control systems and the problem of excessive jitter arrays in traditional sliding mode control, which has better immunity but lags in the tracking of time-varying signals [2826].

This work offers a Compound Variable Structure PI (CVSPI) controller and an upgraded Model Reference Adaptive System (MRAS) speed to increase the control accuracy of the IPMSM speed sensorless speed control system in a wide range of speeds domain. The CVSPI can adjust the inclusion of the integration term, according to the magnitude of the speed error to accelerate the start-up speed. Using the concept of inverse calculation compensation, the estimated rate is input into the anti-integration saturation gain in order to reduce step response exceedance. Additionally, the performance of the tacho loop tracking response is improved by the inclusion of a specified input differential feed-forward connection, which allows for a more precise reaction to input signals that change over time. To address the limitation of the stator current-based MRAS to provide reliable estimates of speed only at moderate and high frequencies, a linear compensation matrix incorporating inductive characteristics substitutes for the unit matrix.

This paper is organized as follows. Section 2 presents the design of the CVSPI and analyses its advantages and performance. Section 3 demonstrates that the linear compensation matrix with inductive parameters satisfies the conditions for Popov super stability and derives a new speed adaptive law. Section 4 carries out simulation experiments and analyses to validate the proposed method. Finally, Section 5 concludes the paper.

2. Composite variable structure PI speed controller

2.1. Design of the composite variable structure PI

The two main anti-windup control methods are limit-stop integration and inverse calculation. The former starts with the nature of the Windup phenomenon in the integration term and chooses to use the integrator action depending on whether the controller output is limited. When the controller is saturated, the integrator action is canceled, and the controller is equivalent to a P control. In contrast, when the controller output is in the

Preprints (www.preprints.org) | NOT PEER-REVIEWED | Posted: 1 September 2022 doi:10.20944/preprints202209.0022.v1

linear region, the integrator action is added to obtain excellent steady-state control performance. However, the generality is poor, and the parameters are selected fixed and challenging to transpose. The latter method reduces the input to the integrator by feeding back the difference between the input and output quantities of the saturated non-linear link to the information of the integrator, thus suppressing the Windup phenomenon. This method has a linear structure, is easy to design, and is a commonly used Anti-Windup control method in engineering today. However, its transient control performance is heavily dependent on the feedback gain rather than the parameters of the PI controller. There is hysteresis, making it difficult to achieve the performance targets of a wide range of motor speed control systems in practice.

To improve the control performance of the speed control system, this paper integrates the advantages of the limit stop integral method and the inverse calculation method and proposes the CVSPI controller shown in Figure 1. The proportion of the integration coefficient to the regulation time in CVSPI can be automatically adjusted depending on the magnitude of the speed deviation. When there is a large speed deviation (i.e., beginning with the motor's maximum acceleration), only the proportional term is used to enter the saturation state; and the integral term is allowed to be added to eliminate the residual difference when the speed error is small (which can be adjusted according to the actual situation).This allows the controller to desaturate early, reducing the overshoot of the response speed, reducing the regulation time, and improving the dynamic response and immunity of the system. The CVSPI enhances the system's dynamic performance based on a simple structure, ensures the control accuracy of the system, enhances the tracking response performance, immunity, and stability of the tacho loop system, and reduces the static and dynamic errors of the system.

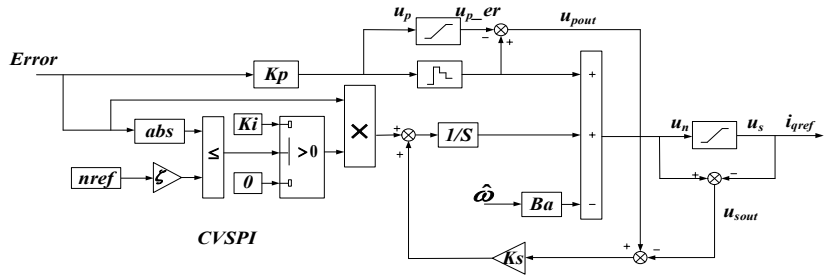

Figure 1. Block diagram of the CVSPI controller architecture.

To address the problem of low accuracy compensation by the integral term alone, CVSPI treats the compensation of the proportional and integral terms separately, significantly reducing the mutual influence of the proportional and integral terms on saturation. This allows the proportional term to be used to its full potential while also enabling Windup suppression, with few changes to the control structure, making it easy to apply. It is possible to achieve a faster and overshoot-free given time while reducing the impact of the Windup phenomenon on system performance. The integration state can be expressed as follows: $\dot{q} = e(t) - K_s(u_{pout} - u_{sout})$, where k_s is the anti-saturation gain.

According to the above equation, selecting the anti-saturation gain is one of the keys to improving system performance. In previous designs, the anti-saturation gain was determined whether the controller output was saturated or not. This method can improve the dynamic system performance at step response, but a fixed anti-saturation gain cannot better suppress the integral saturation at different given speeds. To get the output current out of the saturation state quickly while still being able to respond promptly to changes in the given speed, and adapt to different given rates, it is necessary to combine the operating characteristics of the IPMSM in other states using the inverse calculation idea and introducing the estimated rate of MRAS to automatically adjust the anti-saturation gain. Because of this, the anti-saturation gain is built as equation (1), and its value is set by the motor's specified speed range.

Preprints (www.preprints.org) | NOT PEER-REVIEWED | Posted: 1 September 2022 doi:10.20944/preprints202209.0022.v1

$$K_s = a\hat{\omega} \tag{1}$$

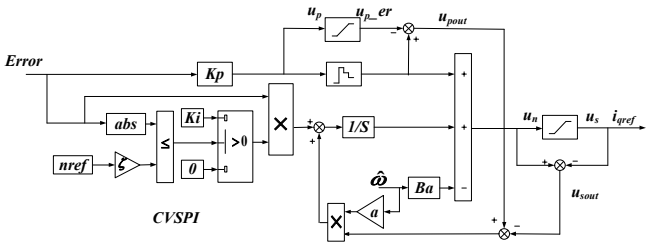

Figure 2. Block diagram of the CVSPI controller architecture.

2.2. CVSPI controller design based on state equations

The IPMSM mechanical equations of motion are:

$$J\frac{d\Omega}{dt} = T_e - T_L - B_a\Omega \quad . \tag{2}$$

Where: T_e and T_L are the motor output electromagnetic torque and load torque respectively;

Ω is the rotor mechanical angular speed;

J is the rotational inertia;

B_a is the viscous friction factor.

The equation of state for mechanical angular velocity is obtained from the above equation:

$$\dot{\Omega} = -\frac{B_a}{J}\Omega + \frac{K_t}{J}i_q^* - \frac{T_d}{J} = -a_s\Omega + b_s i_q^* + d_s(t) \quad . \tag{3}$$

Where: The state factor $a_s = B_a / J$; the control gain $b_s = K_t / J$; i_q^* is the given value of the cross-axis current; the total disturbance torque $T_d = K_t\left(i_q^* - i_q\right) + T_L$, consisting of the disturbance torque due to the current tracking error and the load torque; K_t is the electromagnetic torque factor, $K_t = 1.5p\psi_f$; the disturbance term $d_s(t) = -T_d / J$. Usually, B_a is negligible. So, $a_S \approx 0$. So, the mechanical angular velocity equation of state simplifies to:

$$\dot{\Omega} = b_s i_q^* + d_s(t) \quad . \tag{4}$$

Defining the mechanical angular velocity tracking error $e_s = \Omega^* - \Omega$, the equation of state for the angular velocity tracking error can be obtained as:

$$\dot{e}_s = \dot{\Omega}^* - \dot{\Omega} = \dot{\Omega}^* - b_s i_q^* - d_s(t) \quad . \tag{5}$$

Commonly load disturbances cannot be measured, so a linear proportional-integral feedback control law is required, i.e.:

$$\dot{e}_s = -k_p e_s - k_i \int e_s dt \quad . \tag{6}$$

Where k_p is the scale factor of the controller, and k_i is the integration factor of the controller. Combined (5) and (6) yields a controlled quantity of:

$$i_q^* = \frac{\dot{\Omega}^* + k_p\left(\Omega^* - \Omega\right) + k_i\int\left(\Omega^* - \Omega\right)dt - d_s(t)}{b_s} \quad . \tag{7}$$

Since the equation (2), the actual mechanical angular velocity is usually obtained by differentiating the measured position signal to obtain the angular velocity as feedback. Due to the limited accuracy of the instrument, there is bound to be measurement noise, and the measured position signal is subject to quantization error, further increasing the noise caused by differentiation. Assuming that δ_{ns} is the measurement noise of the

Preprints (www.preprints.org) | NOT PEER-REVIEWED | Posted: 1 September 2022 doi:10.20944/preprints202209.0022.v1

angular velocity and defining the measured mechanical angular momentum as y_s, then we have $y_s = \Omega + \delta_{ns}$. The rotor mechanical angular velocity tracking error then becomes $e_s = \Omega^* - y_s$. Only the CVSPI controller is considered here, so $d_s(t)$ is not directly available and cannot be compensated for, so it is rounded off, and the output torque current is given as:

$$i_q^* = \frac{1}{b_s}\left[\dot{\Omega}^* + k_p\left(\Omega^* - y_s\right) + k_i\int\left(\Omega^* - y_s\right)dt\right] . \tag{8}$$

The actual torque current after limiting is given as:

$$i_{qsat}^* = \begin{cases} i_{q\max}^* \operatorname{sgn}\left(i_q^*\right), & \left|i_q^*\right| > i_{q\max}^* \\ i_q^*, & \left|i_q^*\right| \le i_{q\max}^* \end{cases} . \tag{9}$$

Where i_{qsat}^* is the torque current limit value, and the sgn is the sign function.

In this paper, the CVSPI is supplemented by a given input differential feed-forward link and a control gain link, resulting in a new tacho PI controller, as shown in Figure 3.

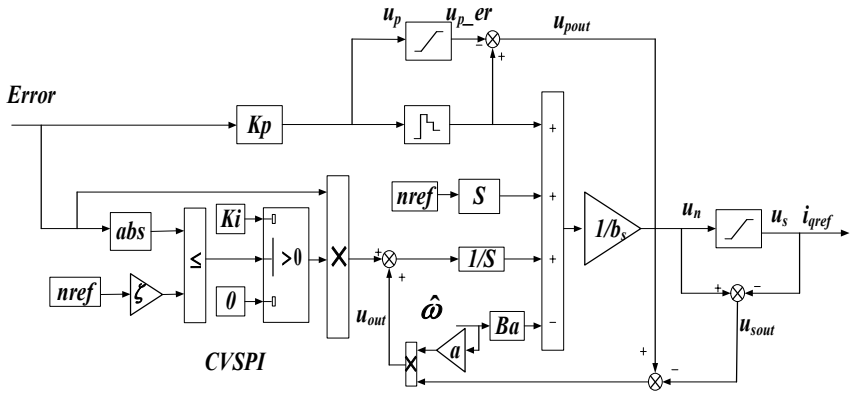

Figure 3. Block diagram of the CVSPI controller architecture.

2.3. Performance analysis of variable structure composite speed controllers

When $error > \zeta nref$,

$$u_s = i_{qsat} . \tag{10}$$

When $error \le \zeta nref$,

$$u_n = \frac{1}{b_s}(k_p e(t) + k_i\int e(t) + a\hat{\omega}\left(u_{pout} - u_{sout}\right)\mathrm{d}t + \frac{d}{dt}nref) . \tag{11}$$

Where: i_{qsat} is the maximum controller output when the system is saturated.

The above equation is for a CVSPI controller with different control structures in the saturation and linear zones. When entering the saturation zone, the motor input current is clamped at a limiting value, allowing the integration state to converge quickly to zero. As the output approaches the linear area, the anti-saturation gain kicks in, allowing the system to enter the linear zone quickly and without overshoot.

As shown in Figure 4, the motor starts with a load running at the rated speed. At the beginning of the start, mechanical inertia deviation is very large, i.e., $error > \zeta nref$, at this time, the integration does not work, relying on the proportional term to make u_n very large, u_s reaches the maximum torque current i_{qsat}, so that the motor starts up with maximum acceleration; at 0.056s, the motor speed reaches 97% of the set speed (can be adjusted according to the actual can), i.e., $error \le \zeta nref$. When the integration link k_i comes into play in the calculation u_n (but does not affect the controller output). At

Preprints (www.preprints.org) | NOT PEER-REVIEWED | Posted: 1 September 2022 doi:10.20944/preprints202209.0022.v1

the same time, the anti-integration saturation module is added to the feedback calculation, and the integration term starts to desaturate. Still, due to the proportional term in the controller, it remains in saturation, making the motor input current still clamped at the limit value, at which point u_n is still greater than u_s , and the speed continues to rise; at 0.0567s due to the estimated speed introduced in the anti-saturation integration gain, the motor speed u_{out} is close to the output of the proportional term u_{p_er} , which is at the desaturation threshold, causing u_{out} to converge rapidly to 0 and u_n to converge quickly to u_s . At this point, the proportional, integral, and inverse calculation compensation links all come into play. The proportional role is small as it is close to the set value and the speed deviation is slight. The integral part is small as it accounts for a smaller proportion of the overall regulation time. u_{out} rapidly decreases close to 0, the speed deviation continues to decline; until the given speed is reached at 0.062s ($u_n = u_s < i_{qsat}$), the controller exits saturation, and the system runs steadily under the sole action of k_i.

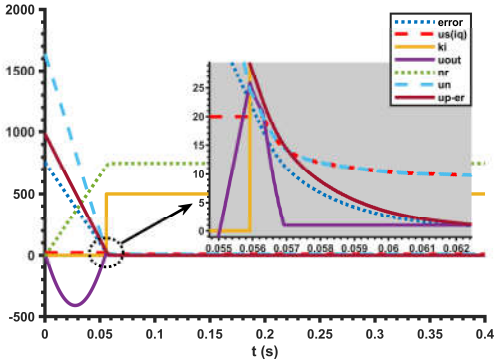

Figure 4. Comparison of the various outputs of the CVSPI controller.

In summary, the above analysis demonstrates that the proportional term acts independently before the minor error, directly making the controller output get the limit value, and the system can begin by the maximum torque current; that at the minor error, the controller quickly exits saturation via the inverse calculation compensation link, thereby improving the system's dynamic performance; and that, via the integral term, the estimated speed and the actual speed are strictly stabilized. Finally, the estimated speed and the actual speed are strictly stabilized at the given speed by the integration term, which improves the static performance of the system and enables the system to reduce speed overshoot while suppressing the integration saturation. The specific parameters of the controller (k_p and k_i) have little effect on the system's dynamic performance, i.e., they are insensitive to the time-varying IPMSM parameters, which improves the system's robustness.

Substitute the equation (8) into the equation (4) to obtain the output of the closed-loop system under CVSPI control as

$$\Omega(s) = \Omega^*(s) + \frac{s}{s^2 + k_p s + k_i} d_s(s) - \frac{k_p s + k_i}{s^2 + k_p s + k_i} \delta_{ns}(s) \quad . \tag{12}$$

When the system has no input differential link, the output of the closed-loop system becomes

$$\Omega(s) = \frac{k_p s + k_i}{s^2 + k_p s + k_i} \Omega^*(s) + \frac{s}{s^2 + k_p s + k_i} d_s(s) - \frac{k_p s + k_i}{s^2 + k_p s + k_i} \delta_{ns}(s) \quad . \tag{13}$$

When the system is given a continuously varying value for the speed input, the control quantity corresponding to its input differential can be responded to in time by the input differential feed-forward link. Combining equation (12), the CVSPI control system

Preprints (www.preprints.org) | NOT PEER-REVIEWED | Posted: 1 September 2022 doi:10.20944/preprints202209.0022.v1

can track continuously varying inputs without steady-state error in the absence of disturbances. When the system is given a constantly varying value for the speed input, the control quantity corresponding to its input differential can be responded to in time by the input differential feed-forward link. Combined with the equation (12), the CVSPI control system can track the continuously varying input without steady-state error in the absence of disturbances. Suppose the input speed is a step signal. In that case, the differential term will be an impulse signal, and the current loop bandwidth and limit will prevent the system's input differential feed-forward link from reacting to the control quantity corresponding to the differential under the step input signal.

In summary, the CVSPI controller, with the addition of a given input differential feed-forward link, is highly immune and robust while simultaneously providing an accurate response to time-varying inputs and enhancing the speed loop tracking response.

3. Improved MRAS speed observer

From the mathematical model of the rotating coordinate system of the built-in permanent magnet synchronous motor:

$$\begin{bmatrix} \frac{di_d}{dt} \\ \frac{di_q}{dt} \end{bmatrix} = \begin{bmatrix} -\frac{R_s}{L_d} & \omega_r \frac{L_q}{L_d} \\ -\omega_r \frac{L_d}{L_q} & -\frac{R_s}{L_q} \end{bmatrix} \begin{bmatrix} i_d \\ i_q \end{bmatrix} + \begin{bmatrix} \frac{u_d}{L_d} \\ \frac{u_q}{L_q} - \omega_r \frac{\psi_f}{L_q} \end{bmatrix} . \tag{14}$$

A reference model from the above equation gives:

$$p\begin{bmatrix} i_d + \frac{\psi_f}{L_d} \\ i_q \end{bmatrix} = \begin{bmatrix} -\frac{R_s}{L_d} & \omega_r \frac{L_q}{L_d} \\ -\omega_r \frac{L_d}{L_q} & -\frac{R_s}{L_q} \end{bmatrix} \begin{bmatrix} i_d + \frac{\psi_f}{L_d} \\ i_q \end{bmatrix} + \begin{bmatrix} \frac{1}{L_d} u_d + \frac{R_s}{L_d^2} \psi_f \\ \frac{1}{L_q} u_q \end{bmatrix} . \tag{15}$$

Where: u_d and u_q are the stator voltages in the $d-q$ reference frame; i_d and i_q are the stator currents in the $d-q$ reference frame; R_s is the stator resistance; ω_r is the rotor electrical pulsation; L_d and L_q represent the stator inductance components in the $d-q$ reference frame; ψ_f is the magnetic flux.

From the equation (15), it can be deduced that:

$$p\begin{bmatrix} i_d^* \\ i_q^* \end{bmatrix} = \begin{bmatrix} -\frac{R_s}{L_d} & \omega_r \frac{L_q}{L_d} \\ -\omega_r \frac{L_d}{L_q} & -\frac{R_s}{L_q} \end{bmatrix} \begin{bmatrix} i_d^* \\ i_q^* \end{bmatrix} + \begin{bmatrix} \frac{1}{L_d} u_d^* \\ \frac{1}{L_q} u_q^* \end{bmatrix} . \tag{16}$$

Where, $i_d^* = i_d + \frac{\psi_f}{L_d}, i_q^* = i_q, u_d^* = u_d + \frac{R_s}{L_d}\psi_f, u_q^* = u_q$.

From the equation (16), it follows that:

$$pi^* = Ai^* + Bu \ . \tag{17}$$

In replacing the equation (17), the speed and current in the equation are replaced by the estimated values to obtain the adjustable model:

$$p\begin{bmatrix} \hat{i}_d^* \\ \hat{i}_q^* \end{bmatrix} = \begin{bmatrix} -\frac{R_s}{L_d} & \hat{\omega}_r \frac{L_q}{L_d} \\ -\hat{\omega}_r \frac{L_d}{L_q} & -\frac{R_s}{L_q} \end{bmatrix} \begin{bmatrix} \hat{i}_d^* \\ \hat{i}_q^* \end{bmatrix} + \begin{bmatrix} \frac{1}{L_d} u_d^* \\ \frac{1}{L_q} u_q^* \end{bmatrix} . \tag{18}$$

Preprints (www.preprints.org) | NOT PEER-REVIEWED | Posted: 1 September 2022 doi:10.20944/preprints202209.0022.v1

Where, $\hat{i}_d^* = \hat{i}_d + \frac{\psi_f}{L_d}, \hat{i}_q^* = \hat{i}_q, u_d^* = u_d + \frac{R_s}{L_d}\psi_f, u_q^* = u_q$.

From the equation (18), it follows that:

$$p\hat{i}^* = \hat{A}\hat{i}^* + Bu \quad . \tag{19}$$

Defining the error vector:

$$e = i_s^* - \hat{i}_s^* \quad . \tag{20}$$

Subtracting the reference model from the adjustable model gives:

$$p\begin{bmatrix} e_d \\ e_q \end{bmatrix} = \begin{bmatrix} -\frac{R_s}{L_d} & \omega_r \frac{L_q}{L_d} \\ -\omega_r \frac{L_d}{L_q} & -\frac{R_s}{L_q} \end{bmatrix}\begin{bmatrix} e_d \\ e_q \end{bmatrix} + (\hat{\omega}_r - \omega_r)\begin{bmatrix} 0 & \frac{L_q}{L_d} \\ -\frac{L_d}{L_q} & 0 \end{bmatrix}\begin{bmatrix} \hat{i}_d^* \\ \hat{i}_q^* \end{bmatrix} \quad . \tag{21}$$

From the equation (21), it follows that:

$$pe = Ae - (\hat{\omega}_r - \omega_r)J\hat{i}_s^* = Ae - W \quad . \tag{22}$$

Where, $W = (\hat{\omega}_r - \omega_r)J\hat{i}^*, A = \begin{bmatrix} -\frac{R_s}{L_d} & \omega_r \frac{L_q}{L_d} \\ -\omega_r \frac{L_d}{L_q} & -\frac{R_s}{L_q} \end{bmatrix}, J = \begin{bmatrix} 0 & \frac{L_q}{L_d} \\ -\frac{L_d}{L_q} & 0 \end{bmatrix}$.

The equation (22) describes a standard non-linear time-varying feedback closed-loop system, applicable to Popov's superstability theory. It consists of a linear constant forward path and a time-varying feedback path. This is seen in Figure 5.

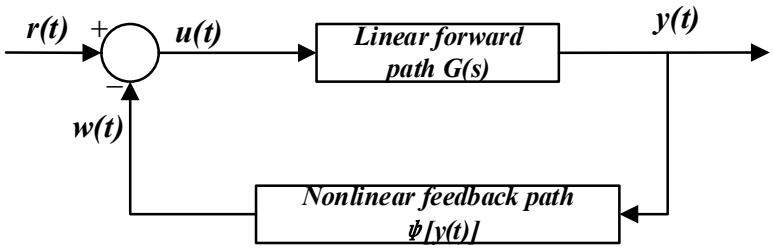

Figure 5. Block diagram of the structure of a non-linear feedback system.

To study the stability of the system shown in Figure 5, assume that $r(t) = 0$, then we have $u(t) = -w(t)$, then the forward pathway can be described as [27]:

$$\begin{cases} \dot{x}(t) = Ax(t) + Bu(t) = Ax(t) - Bw(t) \\ y(t) = Cx(t) + Du(t) = Cx(t) - Dw(t) \end{cases} \quad . \tag{23}$$

The feedback path is :

$$w(t) = \psi[y(t), t, \tau] \tag{24}$$

Where: $x(t)$ is the state variable; $u(t)$ and $y(t)$ are the input and output variables respectively; A is the system matrix; B is the input matrix; C is the output matrix; D is the direct transfer matrix. The forward path selects the matrix C to ensure the system's stability. According to Popov's theorem, the system matrix is given by equations (23) and (24). The sufficient conditions for a system to be asymptotically super-stable are [28]:

1. The transfer function matrix $G(s)$ of the forward path is strictly orthogonal, i.e.:

$$G(s) = D + C(sI - A)^{-1}B \quad . \tag{25}$$

2. The inputs $y(t)$ and outputs $w(t)$ of the feedback path satisfy Popov's inequality:

Preprints (www.preprints.org) | NOT PEER-REVIEWED | Posted: 1 September 2022 doi:10.20944/preprints202209.0022.v1

$$\eta(0,t_1)=\int_0^{t_1} W^T y dt \geq -r_0^{\,2}(\forall t_1>0, r_0^{\,2}\geq 0) \quad . \tag{26}$$

Consequently, the error system derived from the equation (22) can be represented as an equation of state using the equation (23):

$$\begin{cases} pe = Ae - W \\ y = Ce \end{cases} . \tag{27}$$

According to the equation (27), a block diagram of the structure of the error system in Figure 6 is obtained. The solid line is a linear time-invariant (LTI) system. Since the relationship between the output quantity y and the feedback quantity W is uncertain, a non-linear time-varying feedback system (LTV) is used here to represent their relationship.

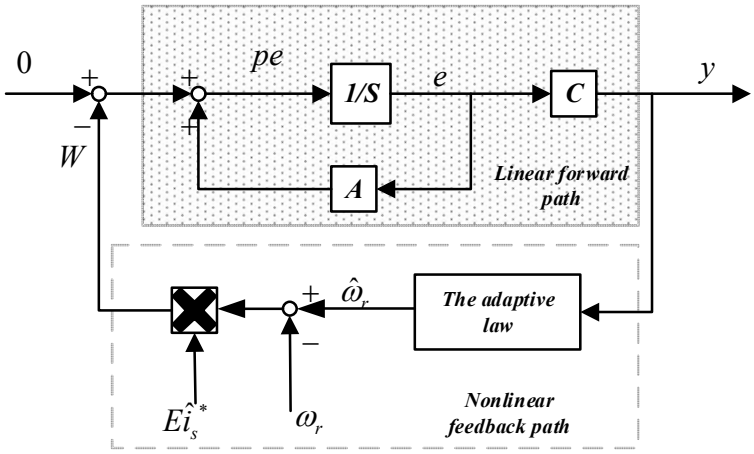

Figure 6. Block diagram of the error system architecture.

For the system shown above to be asymptotically stable, it is necessary to satisfy both equations (25) and (26). For a conventional MRAS, the linear compensation matrix C is set to the unit matrix E. The adaptive law must be redesigned to achieve better speed discrimination over a broad domain.

3.1. Selection of the linear compensator matrix C

The sufficient and necessary conditions for the transfer function matrix $G(s)$ shown in the equation (25) to be a strictly positive real matrix are that there are symmetric positive definite matrices P, Q and real number matrices K, L, and positive actual number λ, which satisfy：

$$\begin{cases} PA + A^T P = -LL^T - 2\lambda P = -Q \\ B^T P + K^T L^T = C \\ K^T K = D + D^T \end{cases} . \tag{28}$$

The equation (22) shows that the B matrix is equal to the unit array, and the D matrix is similar to the zero matrices.

So the equation (28) can be reduced to :

$$\begin{cases} PA + A^T P = -Q \\ P = C \end{cases} . \tag{29}$$

Therefore, $G(s)$ is strictly positive if a reasonable positive definite compensation matrix C is chosen, so that P and Q are positive definite matrices.

Set up: $P=\begin{bmatrix} a_{11} & a_{12} \\ a_{21} & a_{22} \end{bmatrix}, Q=\begin{bmatrix} b_{11} & b_{12} \\ b_{21} & b_{22} \end{bmatrix}$.

Preprints (www.preprints.org) | NOT PEER-REVIEWED | Posted: 1 September 2022 doi:10.20944/preprints202209.0022.v1

Where: $a_{12}=a_{21}$, $b_{12}=b_{21}$. By substituting P and Q into the equation (29):

$$-Q=PA+A^{T}P=$$

$$\begin{bmatrix} -2a_{11}\frac{R_s}{L_d}-2a_{12}\omega_r\frac{L_d}{L_q} & a_{11}\omega_r\frac{L_q}{L_d}-a_{12}(\frac{R_s}{L_q}+\frac{R_s}{L_d})-a_{22}\omega_r\frac{L_d}{L_q} \\ a_{11}\omega_r\frac{L_q}{L_d}-a_{21}(\frac{R_s}{L_q}+\frac{R_s}{L_d})-a_{22}\omega_r\frac{L_d}{L_q} & -2a_{22}\frac{R_s}{L_q}+2a_{12}\omega_r\frac{L_q}{L_d} \end{bmatrix}. \quad (30)$$

Prove the positivity of Q using the trace and determinant of the matrix. The following equation needs to be satisfied:

$$\begin{cases} tr(Q)=b_{11}+b_{22}>0 \\ \det(Q)=b_{11}b_{22}-b_{12}b_{21}>0 \end{cases}. \quad (31)$$

I assume that the new matrix C is: $a_{12}=a_{21}=0, a_{11}=1, a_{22}=\frac{L_q^{\,2}}{L_d^{\,2}}$.

The equation (30) can be reduced to:

$$-Q=\begin{bmatrix} -2\frac{R_s}{L_d} & 0 \\ 0 & -2\frac{L_q}{L_d^{\,2}}R_s \end{bmatrix}. \quad (32)$$

So,

$$\begin{cases} tr(Q)=2*\frac{R_s}{L_d}+2*\frac{L_q}{L_d^{\,2}}*R_s \\ \det(Q)=2*\frac{R_s}{L_d}*2*\frac{L_q}{L_d^{\,2}}*R_s \end{cases}. \quad (33)$$

Clearly, $tr(Q)$ is greater than zero and $\det(Q)$ is greater than zero. So Q is an integer matrix.

So, take:

$$C=P=\begin{bmatrix} 1 & 0 \\ 0 & \frac{L_q^{\,2}}{L_d^{\,2}} \end{bmatrix}. \quad (34)$$

This guarantees the strict validity of $G(s)$.

3.2. *Design of the adaptive law*

Substituting $y=Ce$ and $W=(\hat{\omega}_r-\omega_r)J\hat{i}^{*}$ into $\eta(0,t_1)=\int_0^{t_1}W^{T}ydt\geq -r_0^{\,2}(\forall t_1>0)$ gives:

$$\eta(0,t_1)=\int_0^{t_1}(\hat{\omega}_r-\omega_r)(J\hat{i}^{*})^{T}*Cedt. \quad (35)$$

MRAS parameters are estimated using a proportional integral form, denoted $\hat{\omega}_r$ as:

$$\hat{\omega}_r=\int_0^{t}F_1(y,t,\tau)d\tau+F_2(y,t)+\hat{\omega}_r(0). \quad (36)$$

Where $\hat{\omega}_r(0)$ is the initial value.

Substitute equation (36) into equation (35) to obtain:

Preprints (www.preprints.org) | NOT PEER-REVIEWED | Posted: 1 September 2022 doi:10.20944/preprints202209.0022.v1

$$\begin{aligned}\eta(0,t_1)=\int_0^{t_1}\left[\int_0^t F_1(y,t,\tau)d\tau+\hat{\omega}_r(0)-\omega_r\right]\left(J\hat{i}_s^*\right)^T Cedt+\\ \int_0^{t_1}F_2(y,t)\left(Jy\hat{i}_s^*\right)^T Cedt=\eta_1(0,t_1)+\eta_2(0,t_1)\end{aligned}. \tag{37}$$

To satisfy $\eta(0,t_1)=\int_0^{t_1}W^T ydt\geq -r_0^{\,2}(\forall t_1>0,r_0^{\,2}\geq 0)$, it is possible to make respectively:

$$\eta_1(0,t_1)\geq -r_1^2(r_1\geq 0)\ . \tag{38}$$

$$\eta_2(0,t_1)\geq -r_2^2(r_2\geq 0)\ . \tag{39}$$

For the inequality (38), construct a function $f(t)$ satisfying:

$$\begin{cases}\dfrac{d}{dt}f(t)=\left(J\hat{i}_s^*\right)^T Ce\\ kf(t)=\int_0^t F_1(y,t,\tau)d\tau+\hat{\omega}_r(0)-\omega_r\end{cases}. \tag{40}$$

Where: $k>0$. Substituting equation (40) into equation (38) gives:

$$\eta_1(0,t_1)=\int_0^{t_1}kf(t)\frac{df(t)}{dt}dt=\frac{k}{2}\left[f^2(t_1)-f^2(0)\right]\geq -\frac{k}{2}f^2(0)\geq -r_1^2\ . \tag{41}$$

The derivative of the equation (41) is:

$$k\frac{d}{dt}f(t)=F_1(y,t,\tau)\ . \tag{42}$$

Substitute equation (40) into equation (42) yields:

$$F_1(y,t,\tau)=K_i\left(J\hat{i}_s^*\right)^T Ce\quad(K_i>0)\ . \tag{43}$$

For the equation (39), the inequality must hold if the product function is positive, so take:

$$F_2(y,t)=K_p\left(J\hat{i}_s^*\right)^T Ce\quad(K_p>0)\ . \tag{44}$$

Substitute equation (44) into equation (39) yields:

$$\eta_2(0,t_1)=\int_0^{t_1}K_p\left(J\hat{i}_s^*\right)^T Ce\left(J\hat{i}_s^*\right)^T Cedt\geq 0\geq -r_2^2 \tag{45}$$

Combining equations (41) and (45) into equation (36) yields:

$$\hat{\omega}_r=\int_0^t K_i\left(J\hat{i}_s^*\right)^T Cedt+K_p\left(J\hat{i}_s^*\right)^T Ce+\hat{\omega}_r(0) \tag{46}$$

Where:

$$\begin{aligned}&\left(J\hat{i}_s^*\right)^T Ce=(\hat{i}_s^*)^T J^T Ce\\ &=\begin{bmatrix}\hat{i}_d^* & \hat{i}_q^*\end{bmatrix}\begin{bmatrix}0 & -\dfrac{L_d}{L_q}\\ \dfrac{L_q}{L_d} & 0\end{bmatrix}\begin{bmatrix}1 & 0\\ 0 & \dfrac{L_q^{\,2}}{L_d^{\,2}}\end{bmatrix}\begin{bmatrix}i_d^*-\hat{i}_d^*\\ i_q^*-\hat{i}_q^*\end{bmatrix}=\frac{L_q}{L_d}[\hat{i}_q i_d-i_q\hat{i}_d+\frac{\psi_f}{L_d}(\hat{i}_q-i_q)]\end{aligned}. \tag{47}$$

So, the new speed adaptive law is derived as follows:

$$\hat{\omega}_r=\left(K_p+\frac{K_i}{s}\right)\frac{L_q}{L_d}[\hat{i}_q i_d-i_q\hat{i}_d+\frac{\psi_f}{L_d}(\hat{i}_q-i_q)]+\hat{\omega}_r(0)\ . \tag{48}$$

In summary, the structure of the IPMSM speed control-free speed regulation system is shown in Figure 7.

Preprints (www.preprints.org) | NOT PEER-REVIEWED | Posted: 1 September 2022 doi:10.20944/preprints202209.0022.v1

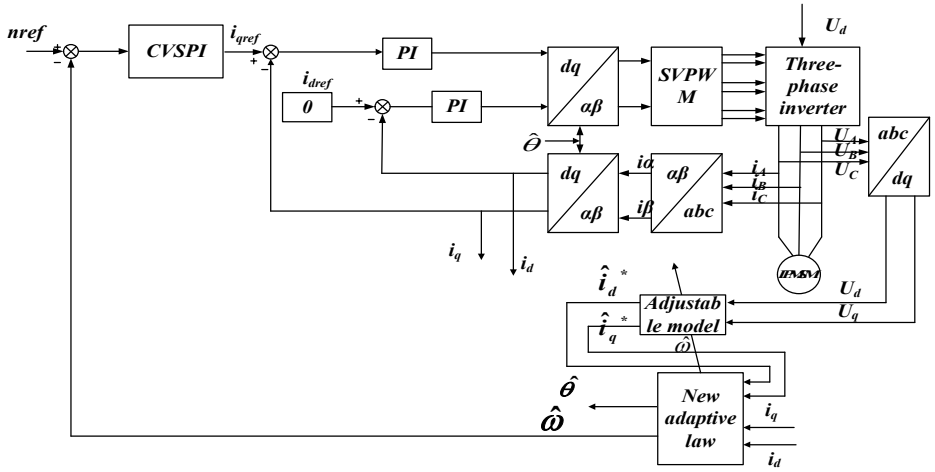

Figure 7. IPMSM speed control system without speed control.

4. Simulation results and analysis

The estimated speed of the MRAS observer proposed in the text is introduced into the system feedback, and an IPMSM simulation platform is built to verify the speed loop control strategy proposed in this paper, demonstrating the high performance of the velocity-free variable frequency speed control system under CVSPI controller. (nref is the given speed, nr is the estimated MRAS speed, and nw is the response speed.) The parameters of the IPMSM used in the simulation are shown below.

Table 1. IPMSM parameters.

Parameters	Value
Rated torque T/(N-m)	25
Rated speed ωref (r/min)	750
Stator resistance Rs/Ω	2.875
Cross-axis inductance Lq/mH	8.5
Straight-axis inductance Ld/mH	8.0
Magnetic flux Ψf/wb	0.175
Polar logarithm Pn	4
Rotational inertia J/(kg-m2)	0.008

4.1. Test of System Dynamic Followership

CVSPI control is compared with the conventional PI controller, anti-windup PI (AWPI) controller proposed in the literature [27], active disturbance rejection controller (ADRC) proposed in the literature [20], and Super-twisting algorithm (STA) proposed in the literature [25] to verify the advantages of the system speed tracking response performance under CVSPI control. nw under five-speed controllers given by sinusoidal speed is shown in Figures 8a and 8c, and the error of nr vs. nw is shown in Figures 8b and 8d. Where the given sine speed is divided into two cases: (i) the peak is 300r/min, the trough is 200r/min, and the frequency is 5 Hz; (ii) the peak is 580r/min, the trough is 520r/min, and the frequency is 15 Hz. When the given sine speed is the first scenario, as shown in figures 8a and 8b, the performance comparison is shown in Table 2.

Preprints (www.preprints.org) | NOT PEER-REVIEWED | Posted: 1 September 2022 doi:10.20944/preprints202209.0022.v1

Table 2. Performance comparison with a peak of 300r/min, a trough of 200r/min, and a frequency of 5hz.

Control strategies	Adjustment time (t/s)	Overshoot	Tracking error (r/min)	Tracking
CVSPI	0.010	None	±0.6	Accuracy
PI	0.015	7.69%	±2.0	Accuracy
AWPI	0.026	None	±1.5	Accuracy
ADRC	0.026	None	±0.8	The estimated speed lags behind the given speed
STA	0.028	None	±0.8	The estimated speed lags behind the given speed

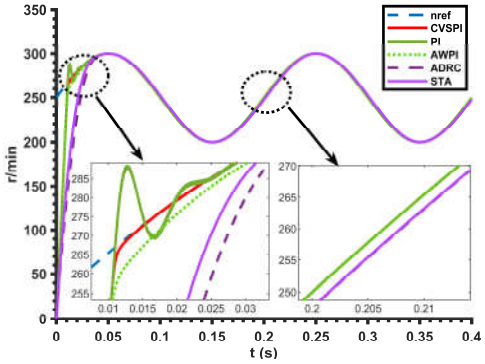

Figure 8a. Estimated and actual rotational speeds for the first sine case.

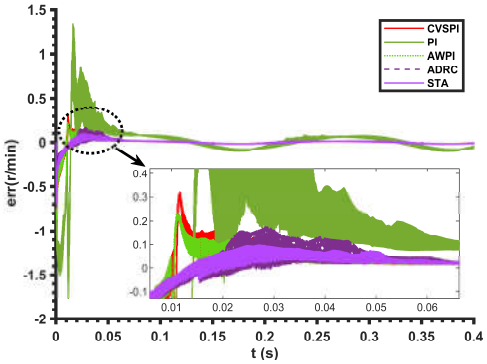

Figure 8b. The Speed error for the first sine case.

Similarly, when the given sine speed is the second case, as shown in Figures 8c and 8d, the performance comparison is shown in Table 3.

Preprints (www.preprints.org) | NOT PEER-REVIEWED | Posted: 1 September 2022 doi:10.20944/preprints202209.0022.v1

Table 3. Performance comparison with a peak of 580r/min and a trough of 520r/min at 15hz.

Control strategies	Adjustment time (t/s)	Overshoot	Tracking error (r/min)	Tracking
CVSPI	0.015	None	±0.6	Accuracy
PI	0.040	5.67%	±2.0	The estimated speed lags behind the given speed
AWPI	0.060	None	±1.5	The estimated speed lags behind the given speed
ADRC	0.060	None	±0.8	The estimated speed lags behind the given speed
STA	0.060	None	±0.8	The estimated speed lags behind the given speed

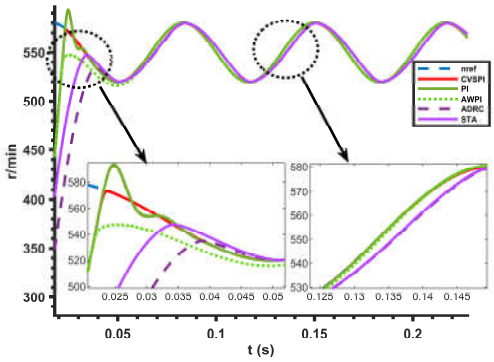

Figure 8c. Estimated and actual rotational speeds for the second sine case.

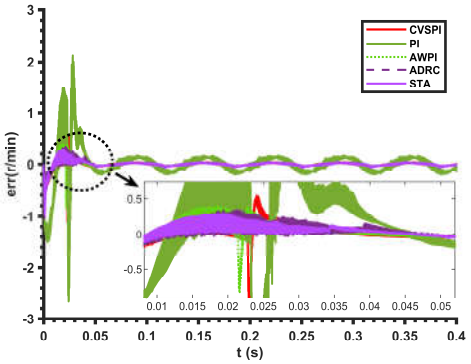

Figure 8d. The Speed error for the second sine case.

It has been demonstrated that CVSPI controller provides a faster and more accurate response to the system feed and can effectively increase the response bandwidth of the system speed loop while also providing better dynamic characteristics.

Preprints (www.preprints.org) | NOT PEER-REVIEWED | Posted: 1 September 2022 doi:10.20944/preprints202209.0022.v1

4.2. Evaluation of System Immunity

By adding and withdrawing loads suddenly at rated speed, we compared the nw of CVSPI controller to that of PI controller, AWPI, ADRC, and STA, validating the advantages of CVSPI controller in terms of resistance to external load disturbance performance. Figure 9a shows the error of nref versus nw for the five-speed controllers at 0.2s with a sudden 15N-m load. The performance comparison is shown in Table 4.

Table 4. Comparison of performance at 0.2s with a sudden 15N-m load at rated speed.

Control strategies	Adjustment time (t/s)	Overshoot	Recovery time (t/ms)	Speed variation under load disturbance
CVSPI	0.030	None	10	10
PI	0.050	7.69%	15	20
AWPI	0.060	None	17	18
ADRC	0.055	None	20	18
STA	0.040	None	30	40

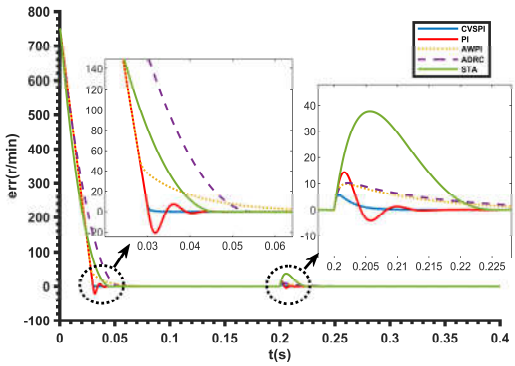

Figure 9a. Speed error during sudden load application.

Figure 9b shows the error of nref versus nw for operation with a load of 15N-m at rated speed for five-speed controllers, with sudden unloading of the load to 5N-m at 0.2s. The performance comparison is shown in Table 5.

Table 5. Comparison of performance with a load of 15N-m at rated speed and a sudden load relief of 5N-m at 0.2s.

Control strategies	Adjustment time (t/s)	Overshoot	Recovery time (t/ms)	Speed variation under load disturbance
CVSPI	0.08	None	10	8
PI	0.12	2.39%	15	18
AWPI	0.12	None	18	15
ADRC	0.06	None	20	15
STA	0.04	None	20	40

Preprints (www.preprints.org) | NOT PEER-REVIEWED | Posted: 1 September 2022 doi:10.20944/preprints202209.0022.v1

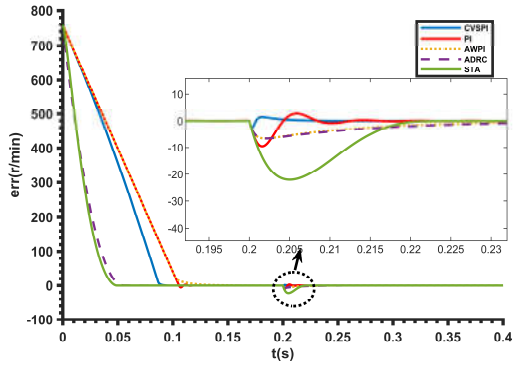

Figure 9b. Speed error during sudden load discharge.

As can be seen from Figures 9a and 9b, the fluctuations in speed response under CVSPI controller are approximately 60% lower than the conventional PI controller, 50% lower than AWPI controller, 48% lower than ADRC controller, and 70% lower than STA controller at the moment of sudden load addition and removal. The steady-state recovery time is also reduced compared to conventional PI, AWPI, ADRC, and STA control. Although CVSPI takes slightly longer than ADRC and STA to reach the rated speed at start-up with load, the CVSPI controller is considerably more resistant to load disturbances than the other controls.

4.3. Evaluation of Systemwide Speed Domain Performance

Under no-load conditions, the high, medium, and low-speed response waveforms and speed estimate waveforms under CVSPI control were compared with the traditional PI, AWPI, ADRC, and STA controller to validate the performance of the CVSPI controller with wide speed domain speed tracking response. The performance of nw and nr for the five-speed controllers at 5 r/min, 15 r/min, 250 r/min, and 750 r/min are shown in Figures 10a to 10e. The performance comparison is shown in Table 6.

Table 6. Comparison of performance in the broad speed domain.

Control strategies	750r/min	250r/min	20r/min	5r/min
CVSPI	Smooth	Smooth	Smooth	Smooth
PI	Overtones	Overtones	Fluctuations	Fluctuations
AWPI	Smooth	Smooth	Overtones	Overtones
ADRC	Smooth	Smooth	Smooth	Jittering
STA	Smooth	Smooth	Smooth	Smooth

Figures 10a–e show that the conventional PI will exhibit large fluctuations in speed response at low speed and evident overshoot at medium and high speed. At the same time, the AWPI can suppress overshoot at high and medium speed better but will show overshoot at low speed, and the ADRC can respond better to different speed situations at both high and low speed, but has poor static stability at low speed (for example, 5r/min). STA can achieve accurate speed following at different speeds. The CVSPI control can be proven superior to the other four controls in attaining performance, high accuracy control of the IPMSM, and a wide speed range with no static stability and fast performance.

Preprints (www.preprints.org) | NOT PEER-REVIEWED | Posted: 1 September 2022 doi:10.20944/preprints202209.0022.v1

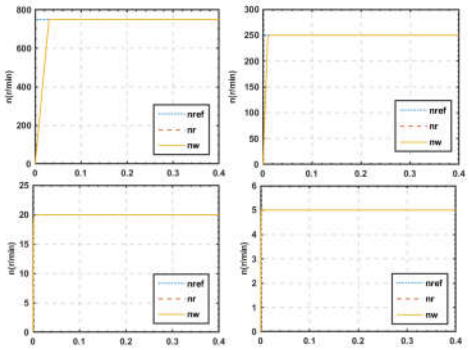

Figure 10a. Estimated speed versus response speed for different speeds of the CVSPI.

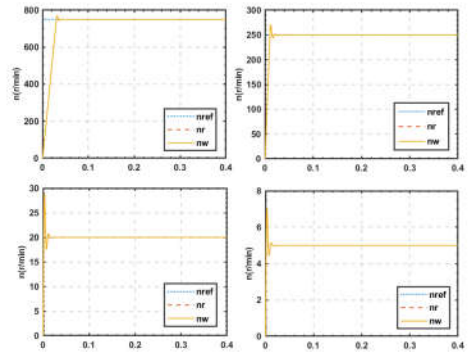

Figure 10b. Estimated speed versus response speed for different speeds of the PI.

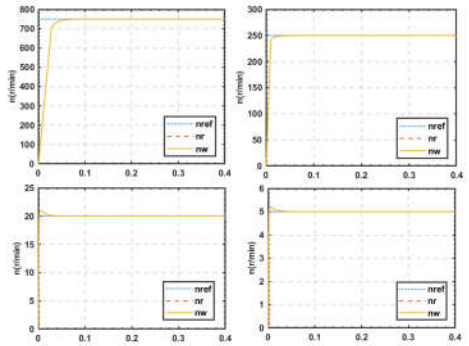

Figure 10c. Estimated speed versus response speed at different speeds of AWPI.

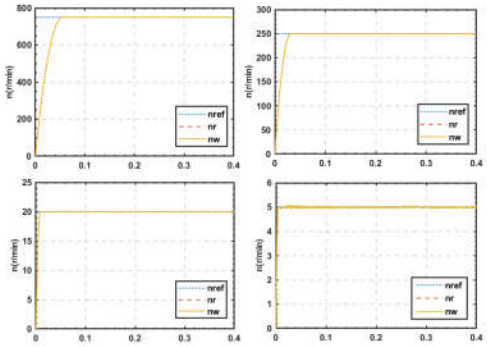

Figure 10d. Estimated speed versus response speed at different speeds of the ADRC.

Preprints (www.preprints.org) | NOT PEER-REVIEWED | Posted: 1 September 2022 doi:10.20944/preprints202209.0022.v1

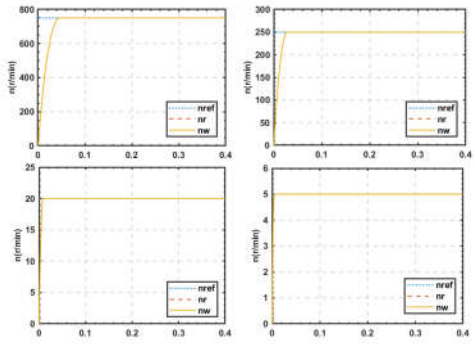

Figure 10e. Estimated speed versus response speed for different speeds of the STA.

4.4. Analyzing the effects of a sudden change in speed while maintaining a consistent torque load

Figure 11 shows the nr waveforms at sudden speed changes under CVSPI, PI, AWPI, ADRC, and STA control, respectively. The motor starts at no load and begins at a given speed of 300r/min, steps from the given speed to the rated speed at 0.2s, drops from the placed speed ramp (slope of -1250) to 500r/min at 0.3s, and steps down to 400r/min at 0.5s. The performance comparison is shown in Table 7.

Table 7. Comparison of step and ramp signal performance.

Control strategies	Step-up stabilisation time (t/ms)	Slopes	Step-down stabilization time (t/ms)
CVSPI	10	Accuracy	10
PI	20, with overshoot	Accuracy	20, with downward overshoot
AWPI	20	Accuracy	50, with a sizeable downward overshoot
ADRC	19	Response speed lags behind the given speed	20
STA	18	Response speed lags behind the given speed	20

Figure 11 shows that the CVSPI controller's nr consistently tracks nref, while the ADRC and STA controllers lag behind the specified speed during the ramp speed provisioning phase; the PI controller experiences a speed response overshoot of 19.8% during this phase; and the AWPI controller experiences a large downward one fluctuation during this phase. The CVSPI controller given in this paper has better dynamic characteristics.

Preprints (www.preprints.org) | NOT PEER-REVIEWED | Posted: 1 September 2022 doi:10.20944/preprints202209.0022.v1

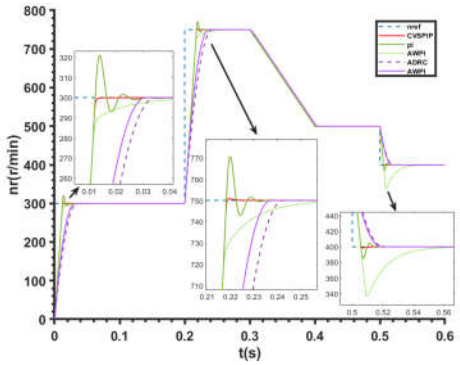

Figure 11. Comparison of the given speed with the actual speed.

5. Conclusions

(1) To minimize or do away with speed overshoot and speed-free control system regulation time, this paper builds on the foundation of the conventional AWPI by integrating the benefits of the encounter limit stop integral method and the inverse calculation method to design a CVSPI controller for use in IPMSM speed-free control systems.

(2) uses the inverse calculation idea to introduce the MRAS estimated speed into the anti-saturation gain to accurately compensate for the system state, enabling the system to quickly exit the integral saturation zone, suppressing the integral saturation phenomenon, and improving the immunity of the system. It also makes the system insensitive to the time-varying motor parameters and improves the system's robustness.

(3) Adding a feed-forward link for a given input differential to accurately respond to time-varying inputs and enhance the speed loop tracking response performance.

(4) CVSPI only requires traditional PI controller parameters and is relatively easy to parameterize.

(5) To enable MRAS to operate efficiently over a wide speed range, a new linear compensator was designed, and a new speed adaptive law was derived.

Simulation results validate that the CVSPI can achieve high performance, high accuracy control, and vast speed domain static differential-free speed regulation of the IPMSM speed-free control system and resolve overshoot of the step response. The response speed and estimated speed under different input signals have good static and dynamic performance. A new approach is provided to study high-performance permanent magnet synchronous motor speed sensorless speed control systems.

Author Contributions: Conceptualization, D.F. and J.B.; methodology, D.F.; software, D.F.; validation, D.F., Z.Z. and J.Z.; formal analysis, D.F.; investigation, D.F.; resources, D.F.; data curation, D.F.; writing—original draft preparation, D.F.; writing—review and editing, D.F.; visualization, D.F.; supervision, J.B.; project administration, J.B.; funding acquisition, J.B. All authors have read and agreed to the published version of the manuscript.

Funding: This research was funded by Jilin Province science and Technology Development Plan project under Grant 20210204116YY.

Acknowledgments: The authors would like to express their gratitude to all those who helped them during the writing of this paper. The authors would like to thank the reviewers for their valuable comments and suggestions.

Conflicts of Interest: The authors declare no conflict of interest.

References

1. Zhang, X.; Tao, R.; Xu, X. et al. Predictive Current Control of a PMSM Three-Level Dual-Vector Model Based on Self-Anti-Disturbance Techniques. *J. Electr. Eng. Technol* **2022**. [https://doi.org/10.1007/s42835-022-01100-8]
2. Zhang, L.; Bai, J; Wu, J. Speed Sensor-Less Control System of Surface-Mounted Permanent Magnet Synchronous Motor Based on Adaptive Feedback Gain Supertwisting Sliding Mode Observer. *Journal of Sensors* **2021,** Article ID 8301359. [https://doi.org/10.1155/2021/8301359]

3. Wang, F.; Li, J. et al., Design of Model Predictive Control Weighting Factors for PMSM Using Gaussian Distribution-Based Particle Swarm Optimization. *IEEE Transactions on Industrial Electronics* **2022**, 69, 10935-10946. [https://doi.org/10.1109/tie.2021.3120441]
4. Liu, Q.; Hameyer, K. High-Performance Adaptive Torque Control for an IPMSM With Real-Time MTPA Operation. *IEEE Transactions on Energy Conversion* 2017, 32, 571-581. [https://doi.org/10.1109/tec.2016.2633302]
5. Liu, Y.; Fang, J., Tan, K.; Huang, B.; He, W. Sliding mode observer with adaptive parameter estimation for sensorless control of IPMSM. *Energies* **2020**, 13, 5991. [https://doi.org/10.3390/en13225991]
6. Liu, K.; Hou, C.; Hua, W. A Novel Inertia Identification Method and Its Application in PI Controllers of PMSM Drives. *IEEE Access* **2019,** 7, 13445-13454. [https://doi.org/10.1109/access.2019.2894342]
7. Hussain, H. A. Tuning and Performance Evaluation of 2DOF PI Current Controllers for PMSM Drives. *IEEE Transactions on Transportation Electrification* **2021,** 7, 1401-1414. [https://doi.org/10.1109/tte.2020.3043853]
8. Kesavan, P.; Karthikeyan, A. Electromagnetic Torque-Based Model Reference Adaptive System Speed Estimator for Sensorless Surface Mount Permanent Magnet Synchronous Motor Drive. *IEEE Transactions on Industrial Electronics* 2020, 67, 5936-5947. [https://doi.org/10.1109/tie.2020.2965499]
9. Khlaief, A.; Boussak, M.; Chaari, A. A MRAS-based stator resistance and speed estimation for sensorless vector controlled IPMSM drive. *Electric Power Systems Research* 2014, 108, 1-15. [https://doi.org/10.1016/j.epsr.2013.09.018]
10. Savitski, D.; Ivanov V.; Augsburg K.; et al. Wheel Slip Control for the Electric Vehicle With In-Wheel Motors: Variable Structure and Sliding Mode Methods. *IEEE Transactions on Industrial Electronics* **2019**, 99, 1-1. [https://doi.org/10.1109/tie.2019.2942537]
11. Tursini M.; Parasiliti F.; Zhang D. Real-time gain tuning of PI controllers for high-performance PMSM drives. *IEEE Transactions on Industry Applications* **2002**, 38, 1018-1026. [https://doi.org/10.1109/tia.2002.800564]
12. Nalepa, R. Generic criterion for tuning of adaptive digital PI current compensators of PMSM drives. *IEEE International Symposium on Industrial Electronics* **2011**, 2011, 601-606. [https://doi.org/10.1109/isie.2011.5984226]
13. Gücin, T. N.; Biberoğlu, M.; Fincan, B.; Gülbahçe, M. O. Tuning cascade PI(D) controllers in PMDC motor drives: A performance comparison for different types of tuning methods. *International Conference on Electrical and Electronics Engineering* **2015**, 2015, 1061-1066. [https://doi.org/10.1109/eleco.2015.7394556]
14. Xiao X.; Li Y.; Li M. Performance control of PMSM drives using a self-tuning PID. *IEEE International Conference on Electric Machines and Drives* **2005**, 2005, 1053-1057. [https://doi.org/10.1109/iemdc.2005.195852]
15. Djelamda, I.; Bouchareb, I.; Lebaroud, A. (2021). High performance hybrid FOC-fuzzy-PI controller for PMSM drives. *European Journal of Electrical Engineering* 2021, 23, 301-310. [https://doi.org/10.18280/ejee.230403]
16. Sarsembayev, B.; Suleimenov, K.; Do, T. D. High Order Disturbance Observer Based PI-PI Control System with Tracking Anti-Windup Technique for Improvement of Transient Performance of PMSM. *IEEE Access* **2021**, 9, 66323-66334. (https://doi.org/10.1109/access.2021.3074661)
17. Repecho,V.; Waqar J.; Biel, D.; et al. Zero speed sensorless scheme for PMSM under decoupled sliding mode control. *IEEE Transactions on Industrial Electronics* **2021**, 99, 1-1. [https://doi.org/10.1109/tie.2021.3062260]
18. Wang Y.; Xu, Y.; Zou, J. Sliding-Mode Sensorless Control of PMSM With Inverter Nonlinearity Compensation. *IEEE Transactions on Power Electronics* **2019**, 2019, 10206-10220. [https://doi.org/10.1109/tpel.2018.2890564]
19. Lu E.; Li, W.; Yang X.; et al. Anti-disturbance speed control of low-speed high-torque PMSM based on second-order non-singular terminal sliding mode load observer. *ISA Transactions* **2018**, 88, 142-152.2018. [https://doi.org/10.1016/j.isatra.2018.11.028]
20. Wang, S. ADRC and Feedforward Hybrid Control System of PMSM. *Mathematical Problems in Engineering* **2013**, 2013, Article ID 180179, 12 pages. [https://doi.org/10.1155/2013/180179]
21. Rong, Z.; Huang, Q. A new PMSM speed modulation system with sliding mode based on active-disturbance-rejection control. *Journal of Central South University* **2016**, 23, 1406. [https://doi.org/10.1007/s11771-016-3193-y]
22. Gai, J.; Huang, S.; Huang, Q.; Li, M.; Wang, H.; Luo, D.; Wu, X.; Liao, W. A new fuzzy active-disturbance rejection controller applied in PMSM position servo system. *International Conference on Electrical Machines and Systems* **2014**, 2014, 2055. [https://doi.org/10.1109/ICEMS.2014.7013842]
23. Roy, P.; Roy, B.K. Dual mode adaptive fractional order PI controller with feed-forward controller based on variable parameter model for quadruple tank process. *Isa Transactions* **2016**, 63, 365-376. [https://doi.org/10.1016/j.isatra.2016.03.010]
24. Gao P.; Zhang, G.; Lv, X. Model-Free Hybrid Control with Intelligent Proportional Integral and Super-Twisting Sliding Mode Control of PMSM Drives. *Electronics* **2020**, 9,1427. [https://doi.org/10.3390/electronics9091427]
25. Liang, D.; Jian, L.; Qu, R. Super-twisting algorithm based sliding mode observer for wide-speed range PMSM sensorless control considering VSI nonlinearity. *IEEE International Electric Machines and Drives Conference* **2017**. [https://doi.org/10.1109/iemdc.2017.8002324]
26. Lee, K.; Ha, J.; Simili, D. Decoupled current control with novel anti-windup for PMSM drives. 2017 *IEEE Energy Conversion Congress and Exposition* **2017**, 2017, 1183-1190. **[**https://doi.org/10.1109/ecce.2017.8095923]
27. Yang M.; Tang, S.; Xu, D. Comments on "Antiwindup Strategy for PI-Type Speed Controller". *IEEE Transactions on Industrial Electronics* **2015**, 62, 1329-1332. [https://doi.org/10.1109/tie.2014.2363626]
28. Turner, M.C.; Sofrony, J.; Prempain, E. Anti-windup for model-reference adaptive control schemes with rate-limits. *Systems & Control Letters* **2020**, 137, 104630. [https://doi.org/10.1016/j.sysconle.2020.104630]